IEEE Access
Multidisciplinary ⋮ Rapid Review ⋮ Open Access Journal

Received 19 February 2024, accepted 26 February 2024, date of publication 1 March 2024, date of current version 12 March 2024.

Digital Object Identifier 10.1109/ACCESS.2024.3371977

RESEARCH ARTICLE

Geometry Design for DOA Estimation in Seismic 2D-Arrays: Simulation Study

NETA ZIMERMAN KATZ[1], MALAAK KHATIB[1], (Student Member, IEEE), YOCHAI BEN-HORIN[2], JONATHAN D. ROSENBLATT[3], AND TIRZA ROUTTENBERG[1], (Senior Member, IEEE)

[1]School of Electrical and Computer Engineering, Ben-Gurion University of the Negev, Be'er Sheva 84105, Israel
[2]Soreq Nuclear Research Center, Yavne 8180000, Israel
[3]Fairmatic, Tel Aviv-Yafo 6721123, Israel

Corresponding author: Malaak Khatib (malaak@post.bgu.ac.il)

This work was supported in part by Israeli Council for Higher Education (CHE) via the Data Science Research Center, Ben-Gurion University of the Negev, Israel; and in part by the PAZY Foundation. The work of Malaak Khatib was supported in part by Paul and Edwina Heller and the Silins Foundation Scholarship, and in part by Israeli CHE Scholarship.

ABSTRACT Sensor array geometry has a direct impact on the direction-of-arrival (DOA) estimation of a seismic signal. In this paper, we design a planar array that aims to optimize the DOA estimation of a narrowband signal in the sense of the minimum mean-squared-periodic-error (MSPE) obtained by the maximum *a-posteriori* (MAP) estimator of the DOA. We investigate the MSPE of the MAP estimator as a main design criterion and compare it with the criteria: 1) the cyclic Bayesian Cramér-Rao bound (CBCRB); and 2) the expected log-likelihood (ELL). The theoretical properties of these criteria are discussed. We show that minimizing the CBCRB is equivalent to maximizing the expected Fisher information matrix. Additionally, maximizing the ELL under a uniform prior is equivalent to minimizing the Kullback-Leibler divergence between the posterior PDF and its estimation. The criteria are compared across three different array geometries, specifically: small arrays, uniform circular arrays (UCAs), and concentric circular arrays (CCAs). Simulation results show that 1) direct MAP-MSPE optimization notably exceeds CBCRB- and ELL-based designs, especially in small arrays; 2) UCAs have suboptimal performance compared to non-circular arrays in many scenarios; 3) under the MAP-MSPE criterion, CCAs match unconstrained design performance with lower computational complexity, making them preferable for smaller arrays; 4) for CCAs and larger UCAs, CBCRB and MAP-MSPE designs yield similar results, while the ELL design excels in the case of small UCAs. Our results highlight the need for selecting suitable array geometries and design criteria in accordance with the scenario and array size in order to achieve the best DOA estimation results.

INDEX TERMS Array design, cyclic Bayesian Cramér-Rao bound (CBCRB), direction-of-arrival (DOA), expected log-likelihood (ELL), minimum mean-squared-periodic-error (MSPE), seismology, seismic array.

I. INTRODUCTION

The direction-of-arrival (DOA) estimation of signals impinging on a sensor array is a well-studied problem in signal processing with a variety of applications, such as communications, radar, and sonar (see, e.g. [1], [2], [3] and references therein), and various solutions have been proposed [4], [5], [6], [7]. In particular, the DOA estimation of a seismic signal can be used to determine the seismic source origin, distinguish between different seismic phases, separate waves from various seismic events, such as earthquakes and human-made explosions, and improve the signal-to-noise ratio (SNR) [8]. The work in [9] delves into specific methodologies and technologies used in array processing for microseismic monitoring. Its focus on advanced signal processing and seismic array technologies contributes to better monitoring and understanding of induced seismicity, thereby improving operational safety and environmental management. DOA

The associate editor coordinating the review of this manuscript and approving it for publication was Hasan S. Mir.

estimation performance is influenced by a number of factors, such as the number of sensors and the antenna directivity. In [10], the impact of antenna directivity and realistic antenna behavior on DOA estimation accuracy was experimentally evaluated. Additionally, improved target localization directly enhances the precision of DOA estimation [11], [12]. The works in [13] and [14] proposed iterative implementation methods that markedly improved source localization accuracy in environments with multipath propagation, and in areas with mixed interference, respectively. Time-difference-of-arrival (TDOA) measurements are widely used to enhance DOA estimation [15], [16]. Moreover, DOA estimation performance strongly depends on the positions of the array sensors. Therefore, careful array design is crucial, subject to physical constraints such as field conditions that may preclude optimum geometries and a limited number of deployed sensors [17]. This paper focuses on optimizing the sensor locations within a seismic planar array for DOA estimation.

In the general array processing literature, the design of arrays based on different criteria has been extensively investigated. For the sparse linear array, different criteria have been proposed in recent years, such as identifiability and recoverability conditions [18]. The work in [19] deals with the optimization of a sparse array in terms of its ability to detect and identify a large number of sources. Optimal sensor geometry for TDOA-based localization has been well-studied in recent years [20], [21]. A large amount of work has been done on designing array geometries by minimizing different variations of the Cramér-Rao Bound (CRB) on DOA estimation [22], [23], [24], [25], [26], [27], [28], [29], [30]. For example, in [31], the stochastic CRB and the asymptotic mean-squared-error (MSE) of the MUSIC algorithm [32] are used to optimize sensor locations in a linear array. The expected CRB (ECRB) and the expected Fisher information matrix (FIM) are suggested as design criteria in [26] and [29]. In [22] and [25], necessary and sufficient conditions on array element locations are found such that the array is isotropic, in the sense that the CRB on the DOA of a single source is uniform for all angles. The advantage of the CRB as an array-design criterion is that it is independent of any particular estimator and, under some conditions, describes the asymptotic performance of the maximum likelihood (ML) estimator [22]. In [33], an analytical method was derived for finding the sparse sensor array that achieves a minimum CRB for the case of one plane wave impinging. In [34], an array geometry for non-circular signals, which increases the aperture for non-circular signals and the number of degrees of freedom for DOA estimation, is presented. However, the CRB does not take into account large estimation errors (outliers) [27], [35]. Outliers constitute a fundamental issue in DOA estimation, and are the result of a large relative height of local maxima in the ambiguity function, i.e. the sidelobe level [36], [37]. Therefore, many CRB-derived designs impose additional constraints to deal with outliers, such as a constraint on the intersensor spacing [27], [28], [29] or on the sidelobe level [24]. However, existing CRB-based methods do not consider the periodic nature of the DOA.

A different approach aims to lower the probability of outliers and ambiguities [3]. Minimization of the probability of gross errors leads to more accurate DOA estimates in low SNR regions. In [38], a measure of similarity between array response vectors is introduced, and a tight lower bound on this similarity measure is suggested as an array-design criterion, where the array with the highest bound has the best ambiguity resolution. Minimization of the expected log-likelihood (ELL) with respect to (w.r.t.) the sensor positions is also described in [39], where the ELL serves as a design criterion due to its relation to the local maxima of the likelihood function and its ability to improve the DOA estimation performance [36].

The seismic literature offers a variety of array-design methods. Seismic arrays are usually designed subject to land topography limitations and use traditional geometries such as the linear, circular, concentric, cross-shaped, or L-shaped geometries [8], [40]. Minimization of the spatial-spectrum estimation error serves as a common design method [41]. Using this method results in a concentric circular geometry, which is a popular seismic array design and is also widely used in other applications [3], [8]. Other works in the seismology literature determine the sensors' positioning in a way that minimizes the influence of ambient noise on array performance, e.g. by constraining zero noise correlation [42] or by maximizing the beamforming SNR gain w.r.t. the sensors' positions [43]. However, these design methods are not specifically focused on improving the DOA estimation performance. The Mount Meron seismic array in northern Israel [44], shown in Fig. 1, is an example of a small aperture array that has motivated this work. Its sensor arrangement, intentionally scattered, is designed to minimize noise correlation between the sensors.

In this paper, we aim to design a planar array that optimizes DOA estimation in the sense of mean-squared-periodic-error (MSPE), which is a natural periodic equivalent of the MSE criterion for periodic estimation problems [45]. The maximum *a-posteriori* (MAP) estimator is commonly used for Bayesian estimation of the DOA, and thus, in practice, we use the numerical MSPE of the MAP estimator as a main design criterion. Since the MAP-MSPE design depends on the specific choice of the estimator and can be only numerically evaluated, it is compared to two other design criteria. The first is a variation of the Bayesian CRB (BCRB), the cyclic BCRB (CBCRB) [46], which considers the periodic nature of the DOA. We show that minimizing the CBCRB criterion is equivalent to maximizing the expected FIM in [26]. We minimize the CBCRB while constraining the outlier probability approximation given in [36], in order to obtain good performance for both small and large error regimes. The second criterion is a Bayesian variation of the

ELL from [39], which aims to reduce outlier occurrence.[1] We prove that under a uniform prior, maximizing the ELL is equivalent to minimizing the Kullback-Leibler divergence (KLD) between the posterior probability density function (PDF) and its estimation. We compare the geometries obtained by the MAP-MSPE, the constrained CBCRB, and the Bayesian ELL, in three examples: 1) a small array with 19 possible locations and 4 available sensors; 2) a uniform circular array (UCA); and 3) a concentric circular array (CCA). The simulations in Section IV are based on the characteristics of the Mount Meron seismic array illustrated in Fig. 1. Results show that the MAP-MSPE design outperforms the CBCRB and ELL designs across all tests performed. Additionally, we highlight the suboptimality of UCAs compared to non-isotropic arrays, whereas CCAs are preferable for larger arrays.

In the rest of this paper we denote vectors by boldface lowercase letters and matrices by boldface uppercase letters. The operators $(\cdot)^T$, $(\cdot)^H$, $(\cdot)^{-1}$, $|\cdot|$, and $\mathrm{Tr}(\cdot)$ denote the transpose, Hermite, inverse, determinant, and trace operators, respectively. The matrix I_M is the identity matrix of order M. The operator $\lfloor\cdot\rfloor$ denotes the floor function. The m^{th} element of the vector a is denoted by a_m. In the following, $\mathbb{E}_x[\cdot]$ and $\mathbb{E}_{x|\theta}[\cdot|\theta]$, denote the expectation and conditional expectation operators given the parameter θ, for any measurable function $A(\cdot)$: $\mathbb{E}_x[A(x)] = \int_{\Omega_x^N} A(x) f_x(x)\,\mathrm{d}x$ and $\mathbb{E}_{x|\theta}[A(x)|\theta] = \int_{\Omega_x^N} A(x) f_{x|\theta}(x|\theta)\,\mathrm{d}x$.

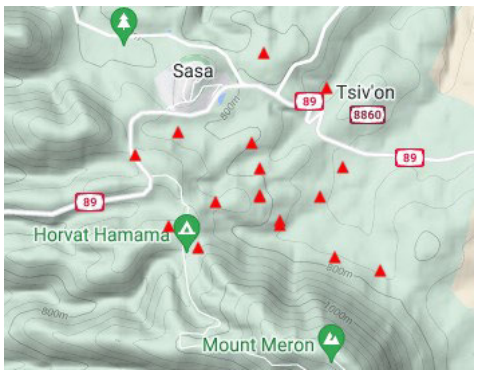

FIGURE 1. Geometry of the Mount Meron seismic array: the red triangles denote the locations of the array sensors that are located near Mount Meron.

II. PROBLEM FORMULATION

In this section, we present the measurements model in Subsection II-A and discuss the MAP estimator and the MSPE as a benchmark for DOA estimation performance of this model in Subsection II-B.

A. MEASUREMENT MODEL

We consider a planar array composed of K sensors located in the x, y plane. We assume a narrowband, far-field, single-source that impinges on the array from the direction given by the azimuth angle $\theta \in [-\pi, \pi)$, named DOA. The measurements model can be described as follows (see, e.g. [1]):

$$x(t_n) = s(t_n)a(Z,\theta) + v(t_n), \quad n = 0,\ldots,N-1, \tag{1}$$

where $s(t_n)$ and $v(t_n)$ are the complex envelope of the signal and of the additive noise, respectively, and $x(t_n)$ contains the measurements from all sensors at time t_n. The steering vector of the kth sensor over the direction θ is defined as

$$[a(Z,\theta)]_k = \exp\left\{-j\frac{2\pi}{\lambda}\left(z_{kx}\sin(\theta) + z_{ky}\cos(\theta)\right)\right\}, \tag{2}$$

$k = 1,\ldots,K$, where $Z = [z_1,\ldots,z_K]^T \in \mathbb{R}^{K\times 2}$ is the augmented matrix of the sensors' positions, in which $z_k = [z_{kx}, z_{ky}]^T$ is the kth sensor location. For the sake of simplicity, we assume that the velocity is known, and therefore the wavelength, λ, is also known. Likewise, for the sake of simplicity, the noise is assumed to be uncorrelated between seismometers in the array, even though this assumption may not hold in practice [49], [50]. The signal $s(t_n)$ and the noise $v(t_n)$ are assumed to be independent identically distributed (i.i.d.), zero-mean, circular, complex, Gaussian random processes with second-order moments $\mathbb{E}_s[s(t_n)s^*(t_n)] = \sigma_s^2$ and $\mathbb{E}_v[v(t_n)v^H(t_n)] = \sigma_v^2 I$, where σ_s^2 and σ_v^2 are the known signal and noise variances, respectively. We assume stationary statistics of the noise and signal during the observation time.

Since our goal is to obtain an array design that is suitable for any DOA, we consider θ to be a random parameter. In particular, since no prior knowledge is available about the DOA, θ is assumed to be uniformly distributed over $[-\pi,\pi)$. In addition, according to the model in (1), it can be verified that the conditional PDF of the observations, x, given the DOA, θ, is

$$f_{x|\theta}(x|\theta) = \frac{1}{\pi^{KN}|R(\theta)|^N} \times \exp\left\{-\sum_{n=0}^{N-1} x^H(t_n)R^{-1}(\theta)x(t_n)\right\}, \tag{3}$$

$\forall\theta \in [-\pi,\pi), x(t_n) \in \Omega_x$, where Ω_x is the observation space, $x \triangleq [x^T(t_0), x^T(t_1),\ldots,x^T(t_{N-1})]^T$, and the covariance matrix is given by

$$R(\theta) = \sigma_s^2 a(Z,\theta)a^H(Z,\theta) + \sigma_v^2 I. \tag{4}$$

The model presented in (1) is periodic w.r.t. the unknown parameter θ, since the array response from (2) satisfies

$$a(Z,\theta) = a(Z,\theta + 2\pi m), \quad \forall m \in \mathbb{Z}. \tag{5}$$

By substituting (4) into (3), we obtain that the *a-posteriori* PDF $f_{x|\theta}(x|\theta)$ is a periodic function w.r.t. θ. Thus, we can properly define a Bayesian periodic parameter estimation problem.

We consider the estimation of the random parameter $\theta \in [-\pi,\pi)$, based on a random observation vector $x \in \Omega_x$,

[1] Not to be confused with the expected likelihood approach in [47] and [48]. In this work, we refer to the ELL as the expectation of the likelihood function.

where Ω_x is the observation space. Let $f_{\theta|x}(\cdot|x)$, $f_{x|\theta}(\cdot|\theta)$, $f_\theta(\cdot)$, $f_x(\cdot)$, and $f_{x,\theta}(\cdot,\cdot)$ denote the *a-posteriori*, conditional, *a-priori*, observation, and joint PDFs, respectively, where $f_{\theta|x}(\varphi|x) = 0$ and $f_\theta(\varphi) = 0$, $\forall\varphi \notin [-\pi,\pi)$. We assume a periodic parameter estimation model where the observation model is periodic w.r.t. the unknown parameters, according to the following definition.

*Definition 1: A Bayesian periodic parameter estimation model is characterized by: 1) a 2π-periodic estimation cost function; and 2) a conditional PDF (*a-posteriori *PDF), $f_{x|\theta}(x|\varphi)$, that is periodic w.r.t. φ with a period $T = 2\pi$, $\forall x \in \Omega_x$.*

B. MSPE OF THE MAP ESTIMATOR

Our goal in this paper is to compare different approaches for choosing the sensor positions, Z, where positions are chosen from a set of possible sensor positions, $\mathcal{Z}$. The positions are chosen in order to improve the performance of the estimation of the DOA in the sense of the MSPE in practical schemes. Thus, we consider here the MAP estimator, which is commonly used for Bayesian estimation of the DOA owing to its tractability and closed-form expression [51].

The MAP estimator is given by

$$\begin{aligned}\hat{\theta}_{\text{MAP}}(x) &\triangleq \arg\max_{\alpha\in[-\pi,\pi)} f_{\theta|x}(\alpha|x)\\ &= \arg\max_{\alpha\in[-\pi,\pi)} \log f_{x|\theta}(x|\alpha),\end{aligned} \tag{6}$$

where $f_{\theta|x}(\alpha|x)$ is the conditional PDF of the DOA, θ, given the observations, x. The last equality in (6) is obtained since the prior is assumed to be uniform (i.e. is a constant $\forall\alpha \in [-\pi,\pi)$), as considered in this paper (see Subsection II-A). By substituting (3) and (4) in (6) and removing constant terms, the MAP estimator in this case is given by [52]

$$\hat{\theta}_{\text{MAP}}(x) = \arg\max_{\alpha\in[-\pi,\pi)} a^H(Z,\alpha)\hat{R}\,a(Z,\alpha), \tag{7}$$

where

$$\hat{R} = \frac{1}{N}\sum_{n=0}^{N-1} x(t_n)x^H(t_n) \tag{8}$$

is the sample covariance matrix. Since θ is uniformly distributed, the estimator in (7) is also the ML non-Bayesian estimator.

In 2π periodic parameter estimation problems, as defined in Definition 1 and such as the DOA problem considered here, only modulo-2π-errors should be considered. As a result, conventional performance criteria, such as the MSE criterion, may lead to absurd results, especially if the unknown state is close to the edges of the circular domain [45]. A commonly-used criterion for periodic parameter estimation is the MSPE, which is the natural periodic-equivalent of the MSE criterion [45]. In this work, we use the MSPE criterion both for performance analysis of the DOA estimation and as a design criterion of the array geometry. The MSPE is calculated as the square of the *modulo* -2π estimation error. The *modulo* -2π operator is defined as[2]

$$\text{mod}_{2\pi}[\varepsilon] = \varepsilon - 2\pi\left\lfloor 0.5 + \frac{\varepsilon}{2\pi}\right\rfloor, \quad \forall\varepsilon\in\mathbb{R}. \tag{9}$$

Thus, for a given DOA estimator, $\hat{\theta} : \Omega_x^N \to [-\pi,\pi)$, the MSPE is given by

$$MSPE(\hat{\theta}) \triangleq \mathbb{E}_{x,\theta}\left[\left(\text{mod}_{2\pi}\left[\hat{\theta}(x)-\theta\right]\right)^2\right]. \tag{10}$$

III. ARRAY DESIGN OPTIMIZATION CRITERIA

In this section, we discuss three design criteria for array geometry. In Subsection III-A we discuss the MSPE of the MAP estimator. The constrained CBCRB and the Bayesian ELL criteria are presented in Subsections III-B and III-C, respectively, as low-complexity alternatives to the MAP-MSPE criterion. For each design criterion, we choose the sensor positions, Z, where the positions are chosen from a set of possible sensor positions, $\mathcal{Z}$.

A. MSPE OF THE MAP ESTIMATOR

In this subsection, we present the MSPE of the MAP estimator as the optimization criterion for array design. For a given DOA estimator, $\hat{\theta} : \Omega_x^N \to [-\pi,\pi)$, the sensor positions that minimize the MSPE are defined as

$$\begin{aligned}Z^* &= \arg\min_{Z\in\mathcal{Z}} \mathbb{E}_{x,\theta}\left[\left(\text{mod}_{2\pi}\left[\hat{\theta}(x)-\theta\right]\right)^2\right]\\ &= \arg\min_{Z\in\mathcal{Z}} \int_{x(t_0)\in\Omega_x}\cdots\int_{x(t_{N-1})\in\Omega_x}\int_{-\pi}^{\pi}\left(\text{mod}_{2\pi}\left[\hat{\theta}(x)-\theta\right]\right)^2\\ &\quad\times\frac{1}{2\pi}f_{x|\theta}(x|\theta)\,\text{d}x(t_0)\ldots\text{d}x(t_{N-1})\,\text{d}\theta,\end{aligned} \tag{11}$$

where $f_{x|\theta}$ is defined in (3) and we substituted the uniform *a-priori* PDF of θ, $f_\theta(\theta) = \frac{1}{2\pi}$, $\forall\theta \in [-\pi,\pi)$. It should be noted that in (11), both the measurements, x, and the covariance matrix, $R(\theta)$, depend on the sensors' locations, Z.

In order to calculate the optimal sensor positions according to (11), a DOA estimator must be chosen. The natural choice is to use the minimum MSPE (MMSPE) estimator [53], which minimizes the MSPE in (10) among all the possible estimators. However, in the general case this estimator is analytically intractable [53]. Thus, we use the MAP estimator, introduced in Subsection II-B, as the estimator for this array design. By substituting (7) in (11), we obtain that the MSPE of the MAP estimator is

$$Z^{\text{MSPE}} = \arg\min_{Z\in\mathcal{Z}} \mathbb{E}_{x,\theta}\left[\left(\text{mod}_{2\pi}\left[\hat{\theta}_{\text{MAP}}(x)-\theta\right]\right)^2\right]. \tag{12}$$

The rationale behind using the MAP-MSPE in (12) as a design criterion is that the MAP estimator is used in practice and not the MMSPE, and that the MSPE is

[2]It should be noted that even when we restrict the estimator to the region $[-\pi,\pi)$, the resulting estimation error can still take values in the region $[-2\pi,2\pi)$.

an appropriate performance measure for DOA estimation. However, calculating Z^{MSPE} exhibits several difficulties, and it is usually analytically intractable. The criteria in the next subsections deal with this intractability. However, it is important to note that, when applicable (e.g. for small arrays), array geometries that result from the design based on the MSPE of the MAP estimator as an optimization criterion can significantly outperform the arrays derived from the commonly used criteria, as we demonstrate in Section IV.

B. CYCLIC BAYESIAN CRAMÉR-RAO BOUND (CBCRB)

In this subsection, we present the sensor array design criterion of the CBCRB. Methods based on the non-Bayesian CRB and the expected FIM for the purpose of array design are widely used in the literature [22], [23], [24], [25], [26], [30]. However, for the Bayesian case, the BCRB itself requires restrictive regularity conditions and usually does not exist in periodic settings. For example, it requires that the *a-priori* PDF of the parameter approaches zero at the endpoints of the parameter support [54]. The CBCRB, which is a cyclic version of the BCRB, was proposed in [45]. The CBCRB was developed as a lower bound on the mean-cyclic-error (MCE) and, in addition, serves as a lower bound on the MSPE, as was shown in [45]. Therefore, it can be used to assess DOA estimation performance and for system design.

The CBCRB for the general case is defined by

$$\mathrm{CBCRB} = 2 - 2\left(1 + \frac{1}{J^{(p)}}\right)^{-\frac{1}{2}}, \tag{13}$$

where

$$J^{(p)} = \mathbb{E}_{x,\theta}\left[\left(\frac{\partial}{\partial\theta}\log f^{(p)}_{x,\theta}(x,\theta)\right)^2\right] \tag{14}$$

is the periodic FIM, in which $f^{(p)}_{x,\theta}$ is a 2π-periodic extension of $f_{x,\theta}$ (for more details see [45]). The CBCRB can be computed even for cases where the BCRB does not exist, such as for a uniform *a-priori* PDF of θ. In particular, it is shown in Appendix A that for a uniform prior PDF over $[-\pi,\pi)$ and a periodic *a-posteriori* PDF, (14) can be written as

$$J^{(p)} = \mathbb{E}_{x,\theta}\left[\frac{\partial}{\partial\theta}\log\left(\frac{1}{2\pi}f_{x|\theta}(x|\theta)\right)^2\right]. \tag{15}$$

In addition, in Appendix B it is shown that the periodic FIM from (15) for the model in (1) is given by

$$J^{(p)} = \frac{N\,\mathrm{SNR}^2}{1+K\,\mathrm{SNR}}\left(\frac{2\pi}{\lambda}\right)^2\left(K\mathrm{Tr}(ZZ^T) - \mathbf{1}^T ZZ^T\mathbf{1}\right), \tag{16}$$

where $\mathrm{SNR} \triangleq \frac{\sigma_s^2}{\sigma_v^2}$. By substituting (16) in (13) we obtain that the CBCRB for the considered model is given by

$$\begin{aligned}\mathrm{CBCRB} &= 2 - 2\\ &\times\left(1 + \frac{1}{\frac{N\,\mathrm{SNR}^2}{1+K\,\mathrm{SNR}}\left(\frac{2\pi}{\lambda}\right)^2\left(K\mathrm{Tr}(ZZ^T) - \mathbf{1}^T ZZ^T\mathbf{1}\right)}\right)^{-\frac{1}{2}}.\end{aligned} \tag{17}$$

Therefore, a design criterion of the array geometry using the CBCRB is given by

$$Z^{\mathrm{CBCRB}} = \arg\min_{Z\in\mathcal{Z}} \mathrm{CBCRB}(Z). \tag{18}$$

Nevertheless, Cramér-Rao type bounds are small-error bounds in the sense that they are achievable (under some conditions) for high SNRs, but are not tight for low values of SNR and/or small numbers of sensors, mainly because they do not take into account the effects of high sidelobes or ambiguity in the directions of the array beampattern. Therefore, design criteria that are based on these bounds should be combined with constraints to avoid array ambiguities or a high sidelobe level that can result in DOA estimation outliers. In particular, we show in the simulations in Section IV that without any constraint the array design obtained by (18) results in poor performance in practice, due to outliers and a small number of sensors. Thus, in order to avoid large estimation errors, a constraint must be applied alongside the CBCRB criterion. Inspired by previous works (see, e.g. [55] and references therein), we use here the probability of an outlier to formulate a constraint on the optimization problem in (18).

It has been shown in [36] that the outlier probability, i.e. the probability that the DOA estimation corresponds with sidelobe maxima, can be approximated by

$$\mathbb{P}[\mathrm{outlier}] \approx \sum_{m=1}^{N_p} \mathrm{P}_m(Z,\theta), \tag{19}$$

where the individual probabilities $\mathrm{P}_m(Z,\theta)$ are the pairwise error probabilities, i.e. the probabilities that the main lobe is lower than sidelobe m. In particular, in our model, these probabilities are given by (see Eq. (22) in [36])

$$\mathrm{P}_m(Z,\theta) = \frac{1}{(1+q_m(Z,\theta))^{2N-1}}\sum_{l=0}^{N-1}\binom{2N-1}{l}q_m^l(Z,\theta), \tag{20}$$

where

$$q_m(Z,\theta) = \frac{\sqrt{1+\frac{4\sigma_v^2(K\sigma_s^2+\sigma_v^2)}{K^2\sigma_s^4(1-r^2(Z,\theta,\theta_m))}}+1}{\sqrt{1+\frac{4\sigma_v^2(K\sigma_s^2+\sigma_v^2)}{K^2\sigma_s^4(1-r^2(Z,\theta,\theta_m))}}-1}, \tag{21}$$

$\{\theta_m\}_{m=1}^{N_p}$ are the beampattern local maxima positions, and $r(Z,\theta,\theta_m) = \frac{|a^H(Z,\theta)a(Z,\theta_m)|}{K}$.

We use the outlier probability in (19) to define the constraint on the CBCRB criterion. The constraint on the outlier probability is given by

$$\max_{\theta\in[-\pi,\pi)} \frac{1}{N_p}\sum_{m=1}^{N_p} \mathrm{P}_m(Z,\theta) \le \varepsilon_0(\mathrm{SNR}), \tag{22}$$

where $0 \le \varepsilon_0(\mathrm{SNR}) \le 1$ is a user-selected threshold, which is calibrated according to the SNR. This is a constraint on the outlier probability for the worst-case scenario w.r.t. θ. Therefore, the constraint is determined according to the largest outlier probability, which is dependent on the DOA angle. To conclude, we define the constrained CBCRB design criterion by

$$\begin{aligned} Z^{\text{Con-CBCRB}} &= \arg\min_{Z\in\mathcal{Z}} \mathrm{CBCRB}(Z) \\ &\text{s.t} \max_{\theta\in[-\pi,\pi)} \frac{1}{N_p}\sum_{m=1}^{N_p} \mathrm{P}_m(Z,\theta) \le \varepsilon_0(\mathrm{SNR}). \end{aligned} \tag{23}$$

Discussion: It can be verified that in the considered setting, the periodic FIM, $J^{(p)}$, in (15) is equal to the expected non-Bayesian FIM in [26], which serves as an array-design criterion. However, it should be noted that the CBCRB serves as a lower bound on the MSPE, where the expected non-Bayesian FIM does not bound the MSPE, and is suggested as an ad-hoc method. The following proposition describes the relation between minimizing the CBCRB and the conventional, deterministic approach.

Proposition 1: Minimization of (13) w.r.t. Z is equivalent to maximization of the expected non-Bayesian FIM for a periodic a-posteriori *PDF and a uniform prior, i.e. where $\theta \sim \mathcal{U}[-\pi,\pi)$, where both terms exist.*

Proof: The proof appears in Appendix A. ■

As a result of Proposition 1, the proposed approach of minimizing the CBCRB gives a new interpretation to the existing method of maximizing the expected FIM with a uniform prior. However, if the prior is not uniform, or if the *a-posteriori* PDF is not a periodic function, then these criteria are different, and it is expected that the constrained CBCRB will lead to a better design for Bayesian DOA estimation.

C. EXPECTED LOG-LIKELIHOOD (ELL)

In this subsection, we propose the Bayesian ELL criterion, which is inspired by the non-Bayesian ELL design criterion suggested in [39]. We define the logarithm of the joint likelihood function as

$$g(Z,\alpha) = \log\left(f_{x,\theta}(x,\alpha)\right), \quad \forall\alpha\in[-\pi,\pi),\ x\in\Omega. \tag{24}$$

Then, the ELL is defined as

$$h(Z,\alpha) \triangleq \mathbb{E}_\theta\Big[\mathbb{E}_{x|\theta}\Big[g(Z,\alpha)|\theta\Big]\Big]. \tag{25}$$

It is important to distinguish between the DOA, θ, and α, which is an arbitrary angle. In Appendix D, it is shown that for the model in (1), $h(Z,\alpha)$ is given by

$$\begin{aligned} h(Z,\alpha) = \frac{\mathrm{SNR}^2\, N}{1+K\ \mathrm{SNR}} \sum_{k,l=1}^{K} I_0\Big(-j\frac{2\pi}{\lambda}\sqrt{\Delta z_{x_{kl}}^2+\Delta z_{y_{kl}}^2}\Big) \\ \times \exp\Big\{j\frac{2\pi}{\lambda}(\sin(\alpha)\Delta z_{x_{kl}}+\cos(\alpha)\Delta z_{y_{kl}})\Big\} + c, \end{aligned} \tag{26}$$

where $\Delta z_{x_{kl}} = z_{kx} - z_{lx}$ and I_0 is the modified Bessel function of the first kind [56, p. 339, sec. 3.338, Eq. (4)] and c is a constant that is independent of α, θ or Z.

The ELL design is obtained by solving a minimax problem on the objective function $h(Z,\alpha)$ defined in (25). That is, according to this design, the sensors' positions are determined by

$$Z^{\text{ELL}} = \arg\min_{Z\in\mathcal{Z}} \max_{\alpha\in[-\pi,\pi)} h(Z,\alpha). \tag{27}$$

The following proposition presents the relation between the ELL and the KLD between the posterior PDF and its estimation.

Proposition 2: Maximizing $\mathbb{E}_{x|\theta}\Big[g(Z,\alpha)|\theta\Big]$ w.r.t. α is equivalent to minimizing the KLD $D_{KL}\Big(f_{x|\theta}(x|\theta)||f_{x|\theta}(x|\alpha)\Big)$ w.r.t. α.

Proof: The proof appears in Appendix E. ■

Proposition 2 implies that the angle that maximizes $h(Z,\alpha)$ is the angle of arrival that describes best the true measurements' PDF. By maximizing (25) w.r.t. α, we minimize the KLD between the two PDFs $f_{x|\theta}(x|\theta)$ and $f_{x|\theta}(x|\alpha)$, and thus, increase their similarity. The motivation for minimizing $h(Z,\alpha)$ w.r.t. Z is related to the array ambiguity and can be explained as follows. We aim to reduce outlier occurrence by minimizing $h(Z,\alpha)$ w.r.t. sensor positions. This may be interpreted as reducing the similarity between the PDFs w.r.t. the sensor positions. Although this is only an intuitive explanation, simulation results in Section IV show that this criterion leads to a design with a relatively low estimation error in the sense of MSPE.

IV. SIMULATIONS

In this section, we present simulation results for different arrays. In Subsections IV-A, IV-B, and IV-C, we consider a small array, a UCA, and a CCA, respectively. It should be noted that the proposed criteria can be applied to additional array configurations, such as sparse linear arrays and uniform linear arrays, by inserting appropriate array shape constraints into the optimization problems.

We evaluate the performance of array geometries obtained by the following methods.

- MAP-MSPE from Subsection III-A - the MAP-MSPE-derived geometry from (12) is determined by using 5,000 Monte Carlo simulations.
- Constrained CBCRB from Subsection III-B - we calculated the left side of (22) for all possible array designs. The value of $\varepsilon_0(SNR)$ from the constrained CBCRB in (23) is set to be the 10th percentile of this

set of values, i.e. 10 percent of all calculated values are below the chosen threshold.
- Bayesian ELL from Subsection III-C.

We evaluate the MSPE performance of the MAP estimator from (7) for each array design that is obtained by the different criteria. Additionally, to further analyze the results, we present the CBCRB of each array by substituting the appropriate Z into (17).

In the following, the measurements were simulated according to the model in Section II-A, with $N = 30$ time samples. We set the wavelength to $\lambda = 1,000$ $[m]$ in order to provide a reasonable ratio to the aperture size and as it represents a value where the array performs best in terms of both sensitivity and wave pattern accuracy (wave velocity and frequency are set to 3000 $[\frac{m}{sec}]$ and 3 $[Hz]$). For each tested case, the performance of the MAP estimator for a given array is evaluated by 5,000 Monte-Carlo simulations.

The sensor array settings in our simulations are based on the characteristics of the Mount Meron seismic array [44], presented in Fig. 1. This includes the wavelength, the number of potential positions, and the grid size for sensor placements, all chosen to align with the specifications of this array. It should be noted that the proposed criteria are broadly applicable to different settings with periodic estimation problems as defined in Definition 1. However for different signal types it is necessary to make specific adjustments, such as aligning the steering vector in (2) to correspond to the signal characteristics and modifying key parameters like the wavelength.

A. DESIGN OF SMALL ARRAY

In this subsection, we consider a small array. Small seismic arrays, especially tripartite arrays, are widely used for seismic recordings for different goals [57]. We denote P as the number of possible sensor positions. Over all possible array geometry combinations and for each design method, the optimal design was found by an exhaustive search. In the following simulations, we use $K = 4$ sensors, $P = 19$ potential locations.[3]

We examine three different values of SNR in order to evaluate the design's robustness to noise. Each of the criteria results in a group of solutions that represent optimal geometries under this criterion. For each criterion, we present a single, arbitrary representative optimal geometry in Fig. 2. First, we note that each criterion results in a different optimal geometry for the different SNR values. It can be seen that the ELL design criterion is independent of the SNR value, as expected from its definition in (27). In addition, we can conclude that the constrained CBCRB design criterion converges at $\sigma_s^2 = 1$. It can be seen that for the MAP-MSPE and constrained CBCRB criteria there is a preference for large distances between the sensors, which aids in the estimation/identification of the angles. We can see that the MAP-MSPE and constrained CBCRB criteria result in different optimal designs; thus, assuming the availability of ample computational power, the MAP-MSPE design should be preferred.

In Fig. 3, We compare the performance of the MAP estimator of the DOA from (7) for the arrays that are obtained using the three design criteria. The performance of the array with locations Z^{CBCRB} that are obtained by minimizing directly the CBCRB in (18) without constraints is also presented, in order to demonstrate the necessity of the constraint in (23). The root MSPE (RMSPE) of the MAP estimator and the root CBCRB of each design are presented in Fig. 3 versus SNR, where the designs for the different criteria are conducted under the assumption that SNR = 0dB. Similar results were obtained for other SNR values. It can be seen that, as expected, the MAP-MSPE design, Z^{MSPE}, has the smallest MSPE at the designed SNR, i.e. at SNR = 0 dB. In addition, when increasing the SNR, Z^{MSPE} still achieves the best performance. When decreasing the SNR, the constrained CBCRB design, $Z^{\text{Con-CBCRB}}$, achieves a slightly lower MSPE, where these two criteria exhibit the best performance compared to the other criteria. Thus, we can conclude that the MAP-MSPE is relatively stable under SNR mismatch. As a result, when optimizing for a small array (i.e. when the computational expense of the MAP-MSPE criterion is acceptable), the MAP-MSPE design, Z^{MSPE}, should be used. In these cases, the MAP-MSPE criterion will lead to the best MSPE performance. For large arrays, when the computation of MAP-MSPE becomes intractable, the constrained CBCRB should be used; although it is not optimal, it provides good performance with a reasonable computation time. Finally, it can be seen that the unconstrained design of Z^{CBCRB} achieves poor results, and the practical MSPE of the MAP estimator with the array obtained by Z^{CBCRB} does not attain its CBCRB bound, even for high SNR values. These results imply that the constraint has a great influence on the optimal geometry, by preferring geometries that are not prone to outliers. It should also be noted that the performance resulting from the MAP-MSPE design, i.e. by Z^{MSPE}, attains its associated CBCRB at the designed SNR, i.e. at SNR = 0 dB. Furthermore, it also attains the CBCRB of the Z^{CBCRB} design, which is a lower bound on the MSPE of all the different scenarios. In theory, the CBCRB of the MAP-MSPE criterion is bounded by the CBCRB of the unconstrained CBCRB criterion, yet for our problem, they coincide. This further supports the MAP estimator choice we made in Subsection III-A. In addition, it can be seen in Fig. 2 that the Z^{ELL} design is independent of the SNR value, while the actual MSPE performance of the MAP estimator for this design depends on the SNR value. Thus, at lower SNRs the associated MAP estimator achieves high MSPE values, but as the SNR increases, its performance attains the associated CBCRB. Furthermore, as the SNR increases, outlier probability decreases and $Z^{\text{Con-CBCRB}}$ and Z^{ELL} produce similar results. The results in Fig. 3 describe the mean estimation performance over all the possible DOAs.

[3]This setting is chosen in accordance with the Mount Meron seismic array (http://www.fdsn.org/networks/detail/IS/) [44], which was also used in [49].

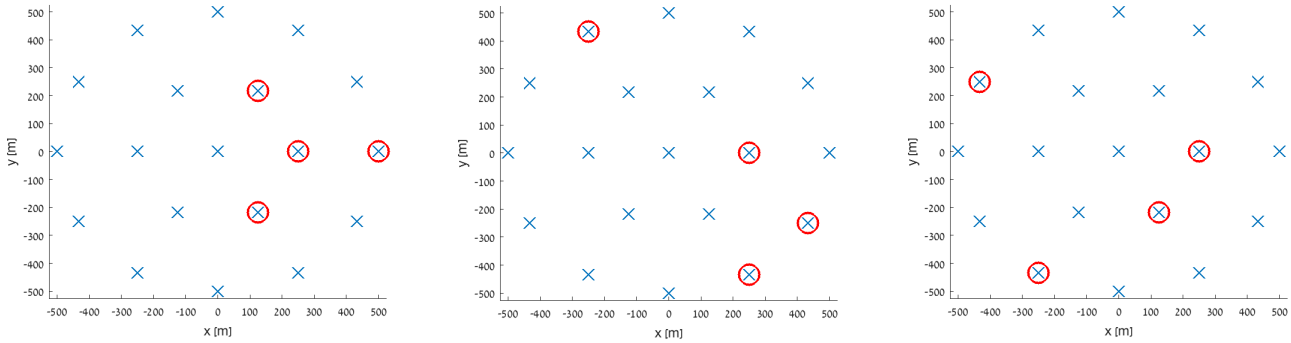

(a1) A member of the $\mathbf{Z}^{\text{MSPE}}$ set (a2) A member of the $\mathbf{Z}^{\text{Con-CBCRB}}$ set (a3) A member of the $\mathbf{Z}^{\text{ELL}}$ set

(a) $\sigma_s^2 = 0.3$

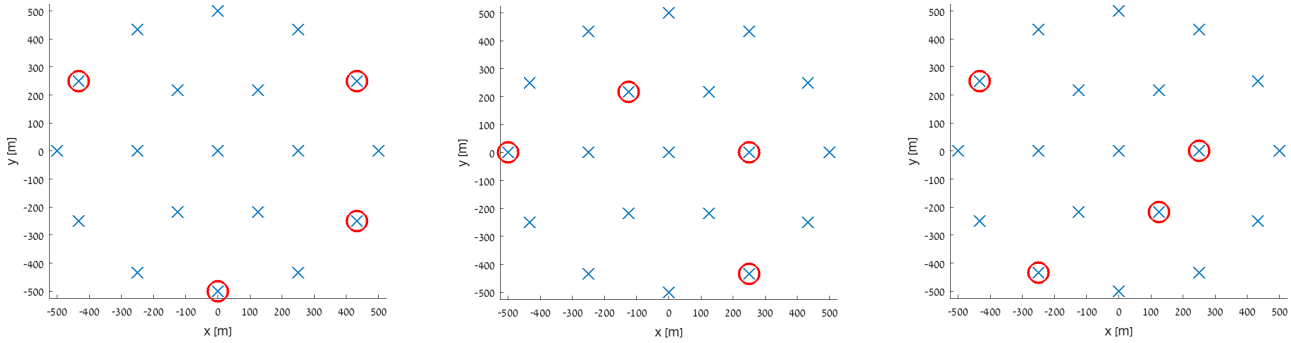

(b1) A member of the $\mathbf{Z}^{\text{MSPE}}$ set (b2) A member of the $\mathbf{Z}^{\text{Con-CBCRB}}$ set (b3) A member of the $\mathbf{Z}^{\text{ELL}}$ set

(b) $\sigma_s^2 = 1$

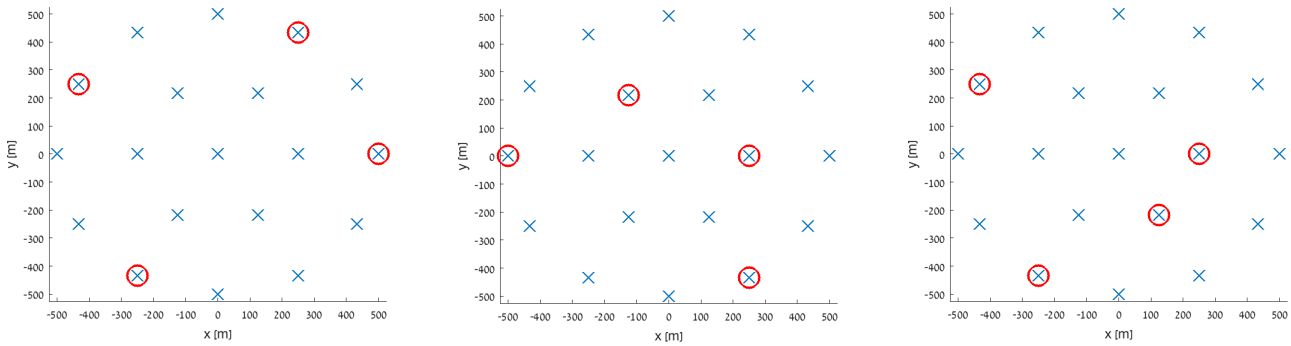

(c1) A member of the $\mathbf{Z}^{\text{MSPE}}$ set (c2) A member of the $\mathbf{Z}^{\text{Con-CBCRB}}$ set (c3) A member of the $\mathbf{Z}^{\text{ELL}}$ set

(c) $\sigma_s^2 = 5$

FIGURE 2. An example of optimal geometries of the sensor array according to the three design criteria for different SNR values, where $\sigma_v^2 = 1$ in all scenarios.

Looking at the accuracy of each DOA estimation is crucial for understanding the strategies behind the different criteria. The arrays are designed to have no preferable direction, which we achieve by defining $\theta \sim \mathcal{U}[-\pi, \pi)$.

In Fig. 4, we present the resultant performance of the different array designs for different DOA values. The number of Monte-Carlo simulations was increased to $50 \cdot 10^3$ for each DOA value and the rest of the simulation parameters were unchanged. The performance is calculated for SNR $=$ 0, 7dB. Firstly, it can be seen that the practical performance of the three criteria is not uniform across the DOAs. In addition, Z^{MSPE} has the best performance for almost every DOA, especially under a high SNR (SNR $=$ 7dB), which corresponds to the conclusion we made regarding Fig. 3

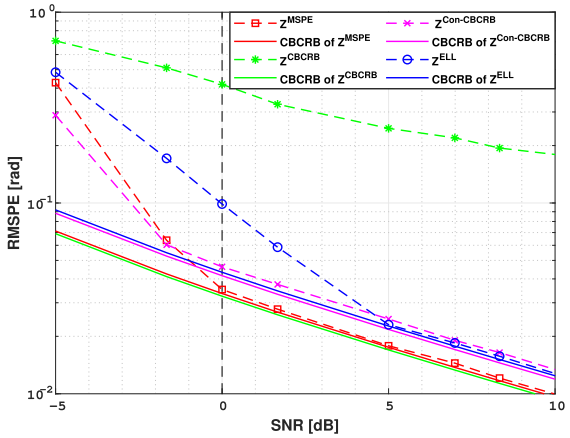

FIGURE 3. **RMSPE versus SNR, designed under** SNR = **0dB. The black vertical dashed line represents the SNR that was assumed during the design process.**

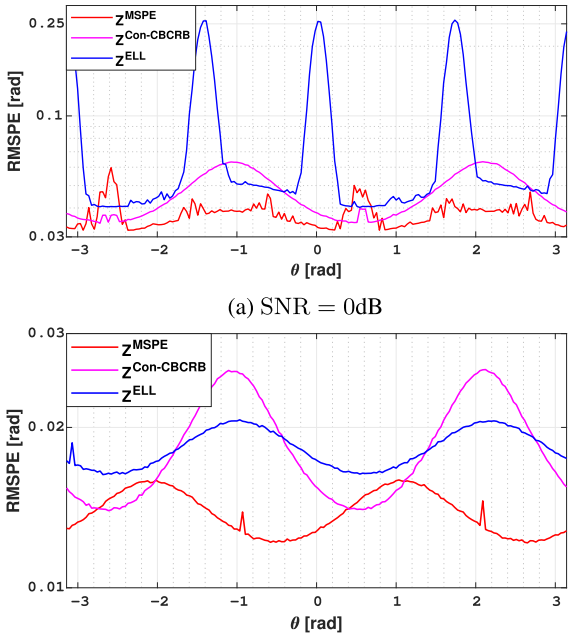

(a) SNR = 0dB

(b) SNR = 7dB

FIGURE 4. **RMPSE versus DOA for (a)** SNR = **0dB and (b)** SNR = **7dB.**

that the Z^{MSPE} design results in the lowest MSPE for an SNR higher than the designed value of SNR = 0dB. For a low SNR (SNR = 0dB), the MSPE of Z^{MSPE} is not as smooth as the MSPE of $Z^{\text{Con-CBCRB}}$ or of Z^{ELL}, which can be explained by the narrower mainlobe of the Z^{MSPE} beampattern. As the SNR increases, both the $Z^{\text{Con-CBCRB}}$ and the Z^{ELL} designs exhibit improved performance, though each excels at different DOA values. However, averaging the performances of the two designs results in an equal mean value of the MSPE, similar to the results in Fig. 3. The $Z^{\text{Con-CBCRB}}$ behavior is dominated by the imposed constraint threshold. Therefore, we ensure a low outlier probability by the constraint threshold. These observations lead to the conclusion that CBCRB and ELL may be poor approximations of the MSPE when the number of sensors is small.

B. UNIFORM CIRCULAR ARRAYS (UCAs)

The UCA is a popular design for DOA estimation since it has uniform performance regardless of the angle of arrival [58], [59]. Therefore, determining the optimal UCA according to the suggested criteria and comparing it to non-UCA configurations are of great interest. In addition, the UCA leads to an optimization procedure with significantly lower computational complexity since the optimization of the different criteria involves only 1D searches on the array radius. In Appendix F, the CBCRB under the UCA assumption is derived, and it is shown that, in this case, Z^{CBCRB} corresponds to the design with the largest radius. As explained in Subsection III-B, the CBCRB alone does not acknowledge the array's ambiguity, and therefor can result in large errors and suboptimal performance without constraints. Under the UCA assumption, the constraint on the CBCRB decreases the optimal (maximal) radius value in order to obtain an outlier probability below some threshold.

In this subsection, we first compare the different criteria for a small UCA ($K = 4$) and for a larger UCA ($K = 20$). In Figs. 5a and 5b we present the results for $K = 4$ and $K = 20$, respectively, where the designs for the different criteria are conducted under the assumption that SNR = 0dB. We consider that the number of optional radii is 50, where the largest possible radius is $r = 500[m]$ (as in Fig. 2), and the rest of the parameters are unchanged. The results for a small UCA are presented in Fig. 5a; it can be seen that, in contrast to the non-UCA constrained arrays in Subsection IV-A where the performance of Z^{ELL} was suboptimal compared to Z^{MSPE} and $Z^{\text{Con-CBCRB}}$, here, Z^{ELL} and Z^{MSPE} exhibit almost the same performance and are favorable over the performance of the $Z^{\text{Con-CBCRB}}$ design. Once again, the MAP-MSPE criterion leads to the optimal overall performance and attains the CBCRB of the MSPE design and of the ELL design. In Fig. 5b it can be seen that for a larger UCA, Z^{MSPE} and Z^{CBCRB} exhibit the same performance, and have the lowest MSPE while attaining the CBCRB across all SNR values. A large number of sensors reduces the outlier probability; therefore, the added constraint to the CBCRB in the $Z^{\text{Con-CBCRB}}$ design is not only no longer crucial, but also leads to worse performance between the different criteria. In this case, the CBCRB is an optimal design criterion, which is also analytically tractable. The outlier probability is reduced significantly to the point that the performance of the estimator resembles its behavior approaching the asymptotic region, i.e. where fine estimation error occurs, and the estimator attains the lower bound. It can be seen that for all the different criteria, the estimator attains the CBCRB for most SNR values. Additionally, in the case of $K = 4$ and $K = 20$, the CBCRB of the MAP-MSPE design was the lowest bound.

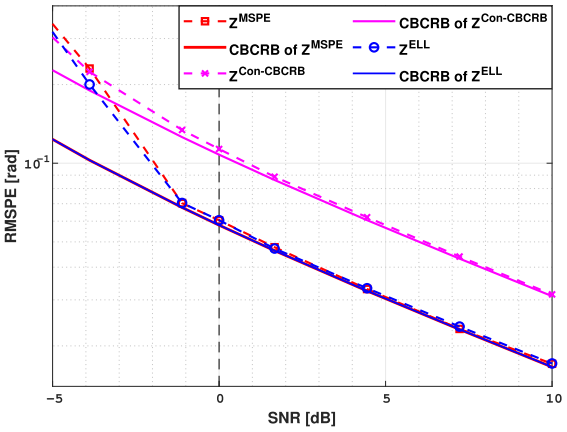

(a) $K = 4$ sensors

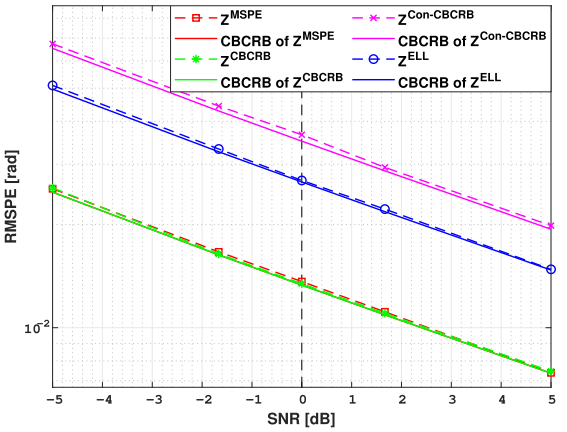

(b) $K = 20$ sensors

FIGURE 5. RMPSE versus SNR for (a) small ($K = 4$ sensors) and (b) large ($K = 20$ sensors) with UCA constraint.

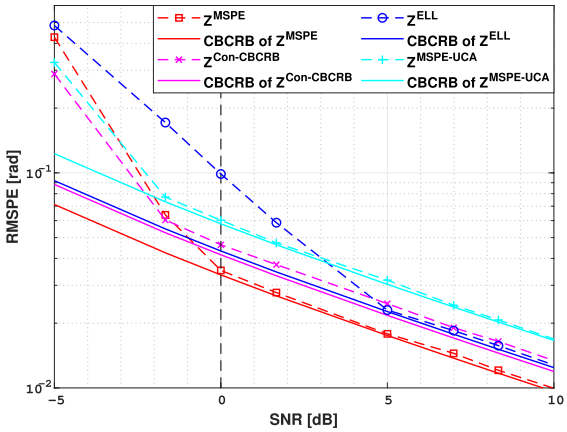

FIGURE 6. RMPSE versus SNR for various design criteria, with UCA constraint.

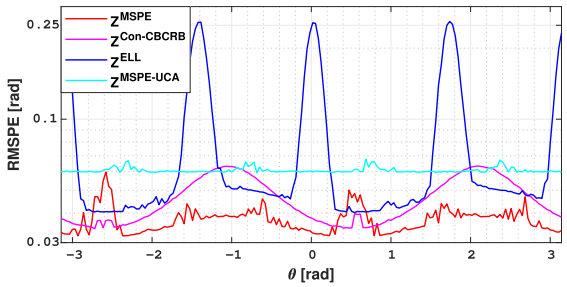

FIGURE 7. RMPSE versus DOA for various design criteria, with UCA constraint.

In the following, the optimal small UCA is compared to arrays derived in Subsection IV-A to show that a UCA constraint may lead to suboptimal performance. We compare the MAP-MSPE design under the UCA constraint, $Z^{\text{MSPE-UCA}}$ (from Fig. 5a), to the MAP-MSPE, constrained CBCRB and ELL designs from Fig. 3. The results are presented in Fig. 6 and Fig. 7. The optimal UCA is chosen from a larger pool of optional positions than the arrays taken from $\mathcal{Z}$ in Fig. 2. It can be observed that $Z^{\text{MSPE-UCA}}$ achieves suboptimal performance compared to Z^{MSPE} and $Z^{\text{Con-CBCRB}}$. Therefore, the UCAs are not part of the optimal geometries set in Subsection IV-A. The suboptimality of the UCA introduced here matches the results obtained in [27], [28], [29], and [60], where it was shown that non-uniform and uniform V-shaped arrays outperform the UCA in the MSE sense, and therefore could outperform the UCA in the sense of MSPE. The non-UCA arrays may have a lower MSPE than the UCA since they exhibit a larger aperture size [60], which is shown in Appendix F to lower the CBCRB. These results show that, in some cases, UCAs are outperformed by a non-isotropic array for almost all DOAs. For these cases, there is no advantage in imposing the UCA constraint.

C. CONCENTRIC CIRCULAR ARRAYS (CCAs)

The concentric circular geometry is a popular seismic array and is widely used in other applications [3], [8], and [41] where this geometry is known to minimize the spatial-spectrum-estimation-error. In this subsection, the concentric circular geometry is examined. First, we derive the optimal CCAs and compare the results for the different criteria.

The design is constrained to be a CCA, with one center sensor and a three-sensor UCA. Then, the array is optimized w.r.t. the UCA radius. The total number of sensors is $K = 4$, and the designs for the different criteria are conducted for SNR $= 0$dB. We consider that the number of optional radii is 50, where the largest possible radius is $r = 500[m]$ (as in Fig. 2), and the rest of the parameters are set as in Subsection IV-A. The results are presented in Fig. 8. It can be seen that Z^{CBCRB} has very similar performance to that achieved by Z^{MSPE}. Therefore, under the simulation settings, the CCA constraint resolves the ambiguity that may occur in some non-constrained geometries. In addition, we can observe that this geometry has isotropic properties that are described through the uniform performance of the four criteria w.r.t. DOA.

In the following, the optimal CCA design is compared to arrays derived in Subsection IV-A. We compare the MAP-MSPE design under the CCA constraint, $Z^{\text{MSPE-CCA}}$, from Fig. 8, to the MAP-MSPE, constrained CBCRB and ELL

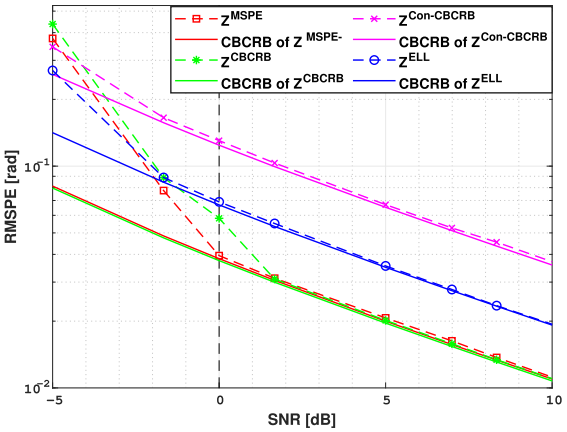

FIGURE 8. RMPSE versus SNR for various design criteria, with CCA constraint.

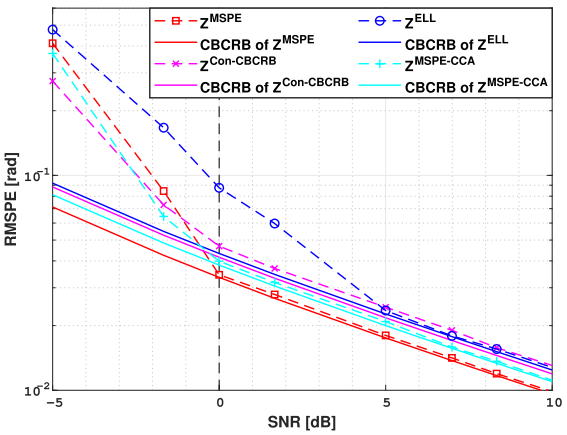

FIGURE 9. RMPSE versus SNR for various design criteria, with CCA constraint.

designs from Fig. 3. The results are presented in Fig. 9 and Fig. 10. It can be seen that the performance of $Z^{\text{MSPE-CCA}}$ is almost indistinguishable from the performance of Z^{MSPE}. For $K = 4$ sensors, $Z^{\text{MSPE-CCA}}$ is determined only by the radius of the outer circle. When increasing the number of sensors, the optimization of a CCA depends on a larger set of parameters, such as the number of outer circles and the number of sensors in each circle. Therefore, the CCA may be a nearly optimal choice for a small geometry, but does not necessarily achieve the minimum MSPE for a large number of sensors.

D. DISCUSSION

In this subsection, we discuss the results obtained in Subsections IV-A-IV-C.

1) SMALL ARRAYS

First, when optimizing for a small array, whether it has a specific shape (i.e. UCA or CCA) or a non-isotropic array, the MAP-MSPE design has the smallest MSPE across all DOAs, as can be seen in Figs. 3, 5a and 8. The performance

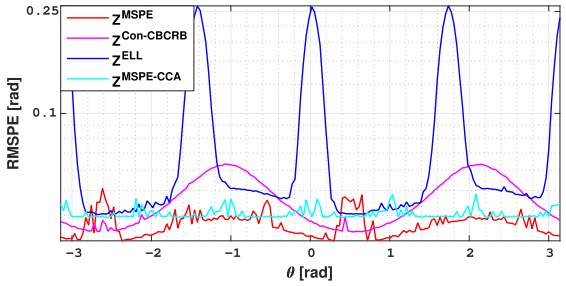

FIGURE 10. RMPSE versus DOA for various design criteria, with CCA constraint.

TABLE 1. The run-time of the different criteria for a UCA with $K = 4, 20$, and 40 sensors..

Criterion	$K = 4$ sensors	$K = 20$ sensors	$K = 40$ sensors
MAP-MSPE	101.1498 [sec]	163.3412 [sec]	248.4957 [sec]
CBCRB	0.003 [sec]	0.0031 [sec]	$3.279 \cdot 10^{-4}$ [sec]
Con-CBCRB	2.2016 [sec]	3.9317 [sec]	5.7544 [sec]
ELL	0.0511 [sec]	0.2633 [sec]	0.5415 [sec]

of the constrained CBCRB and the ELL criteria were suboptimal, especially for an array with a small number of sensors. Moreover, for the MAP-MSPE design, the estimator consistently achieves the CBCRB, indicating its suitability for DOA estimation. It should be noted that when optimizing for a small array or a specifically structured array, such as the UCA, the computational expense of the MAP-MSPE is acceptable. In these cases, the MAP-MSPE criterion should be used, since it will lead to the best MSPE performance. However, when the optimization problem contains a range of sensors, the computation of the MAP-MSPE becomes intractable, and the CBCRB and ELL criteria should be used for arrays with shape constraint (e.g. UCA or CCA), and the constrained CBCRB criterion is advantageous for non-isotropic arrays. The computational complexity of the MAP-MSPE criterion is significantly higher than those of the ELL and the constrained CBCRB criteria since it involves the computation of the MAP estimator for any tested design. To demonstrate the computational cost of using the MAP-MSPE design, we present in Table 1 the run-times for each criterion. The run-time is evaluated using MATLAB on a 4.2 GHz Intel Core i7 iMac with Radeon Pro 575 4 GB and 32 GB DDR4.

It can be seen that in this case, the run-time of calculating the MAP-MSPE design is substantially larger than for the other criteria. Furthermore, the gap between the run-time of the MAP-MSPE design and the other designs increases as the number of sensors increases.

2) UCA, CCA, AND ARBITRARY DESIGN

We compare the performance of the different designs for the UCA with a small ($K = 4$) and a large ($K = 20$) number of sensors. As is shown in Figs. 5a and 5b, in this case, the MAP-MSPE design outperforms the other two criteria. Furthermore, we compare the performance of the

different designs for the UCA and for an array without a shape constraint. We show (see Figs. 6 and 7) that the MAP-MSPE design where we constrained the array to have a UCA shape, achieved suboptimal performance compared to the MAP-MSPE and CBCRB for an unconstrained array. The UCA shaped MAP-MSPE was outperformed by a non-isotropic-array for almost all DOAs, and there is no advantage in imposing the UCA shape in terms of array design.

On the other hand, comparing the MAP-MSPE design under the CCA design with the performance of the three designs for the array with no shape constraint demonstrates (see Figs. 9 and 10) that the MAP-MSPE design exhibits similar performance under both cases and it outperforms the non-isotropic ELL and CBCRB criteria in both cases. The computational complexity of the MAP-MSPE design is lower when considering the CCA shape since it involves optimization over one dimension. Thus, the MAP-MSPE for the CCA may be a nearly optimal choice for a small geometry and should be preferred.

3) CBCRB AND OUTLIERS

We also explore the importance of the outlier probability constraint for the CBCRB criterion. We show that for smaller arrays, the performance of this criterion significantly improves when adding an outlier constraint, but for larger arrays, where the outlier probability decreases substantially, the constrained CBCRB performed worse than any other design, and especially than the non-constrained CBCRB, as is shown in Fig. 5b. In addition, for some shape constraints (e.g. CCA) the outlier probability is reduced, even for smaller arrays; thus the added constraint to the CBCRB design is no longer crucial and worsens the performance of the design, as is seen in Fig. 8. The MAP-MSPE design is more prone to outlier occurrence than the two other design criteria, which can be observed by the results in Fig. 5a. This may be explained by the fact that both the constrained CBCRB and ELL designs aim explicitly to reduce outliers, whereas the MAP-MSPE does not.

4) ELL AND CONSTRAINED CBCRB

The ELL and constrained CBCRB designs are low-complexity alternatives to the MAP-MSPE. The ELL design is independent of the SNR, whereas the constrained CBCRB criterion converges at SNR $=$ 0dB. For non-isotropic small arrays, the constrained CBCRB design results in a lower MSPE than the MAP-MSPE for low SNR values (see Fig. 3). The ELL criterion achieves a notable decrease in MSPE values for high SNR values, performing very similarly to the constrained CBCRB (see Fig. 4b). For UCAs, the ELL design almost achieves the MAP-MSPE design (see Fig. 5a). However, for a larger UCA array, both the ELL and constrained CBCRB were suboptimal. This can be explained by the fact that these two criteria aim to reduce outliers, and for larger arrays, the probability of outliers is significantly lower. In Fig. 8, similar results were obtained for CCA geometries.

V. SUMMARY

In this paper, we consider the problem of optimizing sensor placement, i.e. array design, to improve the DOA estimation of a seismic wave. We proposed the MAP-MSPE criterion for optimal sensor design. Since the parameter estimation has a periodic nature, the MSPE is the relevant objective function in the optimization. In addition, the MSPE of the MAP estimator is chosen as a performance measure, since the MAP estimator is the commonly used method in practice for DOA estimation, owing to its tractability and closed-form expression. We also present the constrained CBCRB and the ELL criteria as low-complexity alternatives to the MAP-MSPE criterion, that are independent of a specific estimation method. We analytically show that 1) minimizing the CBCRB criterion is equivalent to maximizing the expected FIM; and 2) under a uniform prior, maximizing the ELL is equivalent to minimizing the KLD between the posterior PDF and its estimation. To evaluate the performance of the three sensor placement methods, we compare the performance of the MAP estimator resulting from these sensor array designs over small aperture arrays, UCAs, and CCAs. For all these examples and for small and larger arrays, the MAP-MSPE design resulted in overall lower MSPE values. Moreover, under the MAP-MSPE design, the estimator consistently achieves the CBCRB of this design. Furthermore, the CBCRB of the MAP-MSPE is aligned to the lowest bound in every simulation; this corroborates the suitability of this design and the validity of choosing the MAP estimator for this problem. Given the suboptimality of the constrained CBCRB and ELL and current computing power, designing with the MAP-MSPE criterion is an attractive alternative, especially for small arrays that are widely used for seismic recordings [57]. This is also important when large processing power is available, so one can rely on simulation rather than approximations. In addition, we show that UCA and CCA, which are popular geometries due to their isotropic property, are not necessarily optimal in the sense of MSPE. Nevertheless, for a larger number of sensors, concentric circular optimization is more complicated due to the increasing number of inner circles, and CCA designs should be preferred. These conclusions are not limited to seismic arrays and are also valid for other sensor array applications.

Future research could focus on applying the proposed criteria to sparse linear array configurations. This includes implementing tailored methods specifically designed for such arrays, notably nested and coprime arrays. A comparative analysis between these configurations would provide insights and significantly enhance our overall understanding of the distinct performance characteristics of each array type.

APPENDIX A
PERIODIC FIM FOR A UNIFORM PRIOR

In the first part of this appendix, we show that for a uniform prior over $[-\pi, \pi)$ and a periodic estimation problem as defined in Definition 1, the periodic FIM in (14) can

be computed by (15). First, we note that the 2π-periodic extension of a uniform prior PDF w.r.t. θ can be written as

$$f_{\theta}^{(p)}(\theta) = \sum_{l=-\infty}^{\infty} f_{\theta}(\theta + 2\pi l) = \frac{1}{2\pi}, \quad \forall \theta \in \mathbb{R}. \tag{28}$$

In addition, given that the *a-posteriori* PDF is a periodic function w.r.t. θ $\forall x \in \Omega_x$, we obtain that

$$f_{x|\theta}^{(p)}(x|\theta) = f_{x|\theta}(x|\theta).$$

Thus, by using the Bayes rule and the periodic extension in (28), we obtain that the periodic extension of $f_{x,\theta}^{(p)}(x,\theta)$ for a uniform prior (as in the model in Subsection II-A) is given by

$$f_{x,\theta}^{(p)}(x,\theta) = f_{x|\theta}^{(p)}(x|\theta) f_{\theta}^{(p)}(\theta) = \frac{1}{2\pi} f_{x|\theta}(x|\theta), \ \forall \theta \in \mathbb{R}. \tag{29}$$

By substituting (29) into (14), one obtains

$$J^{(p)} = \mathbb{E}_{\theta}\left[\mathbb{E}_{x|\theta}\left[\left(\frac{\partial}{\partial\theta}\log\frac{1}{2\pi} f_{x|\theta}(x|\theta)\right)^2 \Big|\theta\right]\right], \tag{30}$$

which is equal to (15).

The second part of the appendix proves Proposition 1, as follows. We assume that the *a-posteriori* PDF is a periodic function w.r.t. θ, and that θ is uniformly distributed over $[-\pi,\pi)$. Thus, (30) holds, and the internal expectation in (30), $\mathbb{E}_{x|\theta}\left[\left(\frac{\partial}{\partial\theta}\log f_{x|\theta}(x|\theta)\right)^2|\theta\right]$, is equal to the Fisher information for the non-Bayesian estimation of a deterministic unknown parameter, θ, if all the regularity conditions of the BCRB and the non-Bayesian Fisher information hold. Therefore, in cases where $J^{(p)}$ is well defined, θ has a uniform prior over $[-\pi,\pi)$, and the *a-posteriori* PDF is a periodic function w.r.t. θ, $J^{(p)}$ is equal to the expected non-Bayesian Fisher information. Thus, in these cases, maximizing $J^{(p)}$, is equivalent to maximizing the expected non-Bayesian FIM, which proves Proposition 1.

APPENDIX B
PERIODIC FIM CALCULATION

In this appendix, we develop the periodic FIM for the model in (1), and show that it is given by (16). By substituting (3) in the internal expectation in (30), we obtain

$$\begin{aligned}
&\mathbb{E}_{x|\theta}\left[\left(\frac{\partial}{\partial\theta}\log f_{x|\theta}(x|\theta)\right)^2\Big|\theta\right] \\
&= \frac{2N\ K\ \mathrm{SNR}^2}{1+K\ \mathrm{SNR}} \\
&\quad\times\left(\frac{2\pi}{\lambda}\right)^2\sum_{k=1}^{K}\left(z_{kx}\cos(\theta) - z_{ky}\sin(\theta)\right)^2 - \frac{1}{K} \\
&\quad\times\sum_{k,l=1}^{K}\left(z_{kx}\cos(\theta) - z_{ky}\sin(\theta)\right)\left(z_{lx}\cos(\theta) - z_{ly}\sin(\theta)\right),
\end{aligned} \tag{31}$$

where $\mathrm{SNR} = \frac{\sigma_s^2}{\sigma_v^2}$. (31) was obtained using the trace operator and the measurement covariance,

$$\mathbb{E}_{x|\theta}\left[x(t_n)x^H(t_n)\big|\theta\right] = \sigma_v^2 I + \sigma_s^2 a(Z,\theta)a^H(Z,\theta), \tag{32}$$

and the property in [61, Eq. (160)] described by

$$\begin{aligned}
&\left(I + \mathrm{SNR}\ a(Z,\theta)a^H(Z,\theta)\right)^{-1} \\
&\qquad = I - \frac{\mathrm{SNR}\ a(Z,\theta)a^H(Z,\theta)}{1+K\ \mathrm{SNR}}.
\end{aligned} \tag{33}$$

The result in (31) was obtained in various papers (see, e.g. [62]) since $\mathbb{E}_{x|\theta}\left[\left(\frac{\partial}{\partial\theta}\log f_{x|\theta}(x|\theta)\right)^2|\theta\right]$ is equal to the Fisher information under the linear Gaussian model for the estimation of a deterministic θ. Substituting (31) in (30) and using the fact that θ has a uniform prior PDF in $[-\pi,\pi)$ results in

$$\begin{aligned}
J^{(p)} = \frac{2N\ K\ \mathrm{SNR}^2}{1+K\ \mathrm{SNR}}\left(\frac{2\pi}{\lambda}\right)^2\Bigg[&\sum_{k=1}^{K}\left(z_{kx}^2 + z_{ky}^2\right) \\
&- \frac{1}{K}\sum_{k,l=1}^{K}\left(z_{kx}z_{lx} + z_{ky}z_{ly}\right)\Bigg].
\end{aligned} \tag{34}$$

Finally, by substituting $Z = [z_1,\ldots,z_K]^T$, where $z_k = [z_{kx}, z_{ky}]^T$, $k = 1,\ldots,K$, in (34) and using the properties of the trace operator, it can be verified that the result in (34) can be rewritten as (16).

APPENDIX C
ELL CRITERION FOR DETERMINISTIC DOA

In this appendix, we show that when assuming a deterministic θ, the objective functions in [39, Eq. (25a)] and in Section III-C coincide. In [39], the objective function for the purpose of sensor placement is denoted by $|H(\sin(\theta),\cos(\theta),Z)|$, where $H(\sin(\theta),\cos(\theta),Z)$ is the Fourier transform of the spatial sampling pattern and is given by

$$\begin{aligned}
&H(\sin(\theta),\cos(\theta),Z) \\
&\qquad = \sum_{k=1}^{K}\exp\left\{-j\frac{2\pi}{\lambda}[\sin(\theta),\cos(\theta)]z_k\right\}.
\end{aligned} \tag{35}$$

We show that taking the inner expectation in (26) results in the same objective function as in [39]. The conditional distribution of the measurements model in Section II-A w.r.t. θ is given by

$$\begin{aligned}
&f_{x|\theta}(x|\theta=\alpha) \\
&= \prod_{n=0}^{N-1}\frac{1}{\pi^k|\sigma_v^2 I + \sigma_s^2 a(Z,\alpha)a^H(Z,\alpha)|} \\
&\quad\times\exp\left\{-x^H(t_n)\left(\sigma_v^2 I + \sigma_s^2 a(Z,\alpha)a^H(Z,\alpha)\right)^{-1}x(t_n)\right\}.
\end{aligned} \tag{36}$$

Using the property in [61, Eq. (24)] described by

$$\left|I + \text{SNR} - a(Z,\theta)a^H(Z,\theta)\right| = 1 + K\ \text{SNR} \tag{37}$$

and (33), and by taking the logarithm of (36) and writing the expressions which are not dependent on α and Z as a constant c, we obtain the following expression

$$g(Z,\alpha) = \frac{\text{SNR}}{\sigma_v^2 + K\ \sigma_s^2}\ a^H(Z,\alpha) \times \sum_{n=0}^{N-1} x(t_n)x^H(t_n)a(Z,\alpha) + c, \tag{38}$$

$\forall\alpha \in [-\pi,\pi)$. From this point, we treat $g(Z,\alpha)$ as a likelihood function, where α is a search parameter, and θ is the true deterministic DOA. The conditional expectation of $g(Z,\alpha)$ given θ is

$$\mathbb{E}_{x|\theta}\Big[g(Z,\alpha)\big|\theta\Big] = \frac{N\ \text{SNR}}{\sigma_v^2 + K\ \sigma_s^2} \times a^H(Z,\alpha)\Big(\sigma_v^2 I + \sigma_s^2 a(Z,\theta)a^H(Z,\theta)\Big)a(\alpha,Z). \tag{39}$$

With some algebra, we obtain

$$\begin{aligned}&\left|\left|a^H(Z,\theta)a(Z,\alpha)\right|\right|_2^2 \\ &= \sum_{k,l=1}^{K} \exp\Big\{-j\frac{2\pi}{\lambda}\Big[\big(\sin(\theta) - \sin(\alpha)\big)\Delta z_{x_{kl}} + \big(\cos(\theta) - \cos(\alpha)\big)\Delta z_{y_{kl}}\Big]\Big\} \\ &= \Big|H\big(\sin(\theta) - \sin(\alpha), \cos(\theta) - \cos(\alpha), Z\big)\Big|^2,\end{aligned} \tag{40}$$

where $\Delta z_{x_{kl}} = z_{xk} - z_{xl}$. Using (40), (39) is given by

$$\begin{aligned}&\mathbb{E}_{x|\theta}\Big[g(Z,\alpha)\big|\theta\Big] \\ &= \frac{K\ \text{SNR}\ N}{1 + K\ \text{SNR}} + \frac{\text{SNR}^2\ N}{1 + K\ \text{SNR}} \times \sum_{k,l=1}^{K} \exp\Big\{-j\frac{2\pi}{\lambda}\Big[\big(\sin(\theta) - \sin(\alpha)\big)\Delta z_{x_{kl}} + \big(\cos(\theta) - \cos(\alpha)\big)\Delta z_{y_{kl}}\Big]\Big\} + c \\ &\sim \Big|H\Big(\sin(\theta) - \sin(\alpha), \cos(\theta) - \cos(\alpha), Z\Big)\Big|^2.\end{aligned} \tag{41}$$

Therefore, assuming that the DOA is a deterministic parameter and the conditional distribution in (36), the ELL design criterion presented in this paper coincides with the design criterion in [39].

APPENDIX D
ELL DERIVATION FOR OUR MODEL

In Appendix C, we obtained $\mathbb{E}_{x|\theta}\big[g(Z,\alpha)|\theta\big]$ in (41), where c is a constant that encapsulates the expressions that are independent of α and Z. We will perform $\mathbb{E}_\theta\Big[\mathbb{E}_{x|\theta}\big[g(Z,\alpha)|\theta\big]\Big]$, and again denote by c the expressions that are not dependent on θ:

$$\begin{aligned}&\mathbb{E}_\theta\Big[\left|\left|a^H(Z,\alpha)a(Z,\theta)\right|\right|_2^2\Big] + c \\ &= c + \frac{1}{2\pi} \times \int_{-\pi}^{\pi} \sum_{k,l=1}^{K} \exp\Big\{-j\frac{2\pi}{\lambda}\Big[(\sin(\theta) - \sin(\alpha))\Delta z_{x_{kl}} + (\cos(\theta) - \cos(\alpha))\Delta z_{y_{kl}}\Big]\Big\}\,\mathrm{d}\theta = c + \frac{1}{2\pi} \\ &\times \sum_{k,l=1}^{K} \exp\Big\{j\frac{2\pi}{\lambda}\big(\sin(\alpha)\Delta z_{x_{kl}} + \cos(\alpha)\Delta z_{y_{kl}}\big)\Big\} \times \int_{-\pi}^{\pi} \exp\Big\{-j\frac{2\pi}{\lambda}\big(\sin(\theta)\Delta z_{x_{kl}} + \cos(\theta)\Delta z_{y_{kl}}\big)\Big\}\,\mathrm{d}\theta \\ &= c + \sum_{k,l=1}^{K} I_0\Big(-j\frac{2\pi}{\lambda}\sqrt{\Delta z_{x_{kl}}^2 + \Delta z_{y_{kl}}^2}\Big) \times \exp\Big\{-j\frac{2\pi}{\lambda}\big(\sin(\alpha)\Delta z_{x_{lk}} + \cos(\alpha)\Delta z_{y_{lk}}\big)\Big\},\end{aligned} \tag{42}$$

where $\Delta z_{x_{kl}} = z_{xk} - z_{xl} = -\Delta z_{x_{lk}}$ and I_0 is the modified Bessel function of the first kind [56, p. 339, sec. 3.338, Eq. (4)].

APPENDIX E
PROOF OF PROPOSITION 2

In this appendix, we prove Proposition 2, which relates the ELL criterion and the KLD. The KLD [63] is given by

$$\begin{aligned}&\mathrm{D_{KL}}\Big(f_{x|\theta}(x|\theta)||f_{x|\theta}(x|\alpha)\Big) \\ &= \mathbb{E}_{x|\theta}\left[\log\left(\frac{f_{x|\theta}(x|\theta)}{f_{x|\theta}(x|\alpha)}\right)|\theta\right] \\ &= \int_{\Omega_x^N} \log\left(\frac{f_{x|\theta}(x|\theta)}{f_{x|\theta}(x|\alpha)}\right) f_{x|\theta}(x|\theta)\,\mathrm{d}x,\end{aligned} \tag{43}$$

where θ is defined to be the true, unknown DOA, and α is the estimated arrival angle. Using (33) and (37), and substituting the conditional distribution in (36) into (43), the $\mathrm{D_{KL}}$ for the presented model in Subsection II-A is given by

$$\begin{aligned}&\mathrm{D_{KL}}\Big(f_{x|\theta}(x|\theta)||f_{x|\theta}(x|\alpha)\Big) \\ &= \frac{\text{SNR}}{\sigma_v^2 + K\ \sigma_s^2}\mathbb{E}_{x|\theta}\Big[\sum_{n=0}^{N-1} x^H(t_n) \times \Big(a(Z,\theta)a^H(Z,\theta) - a(Z,\alpha)a^H(Z,\alpha)\Big)x(t_n)\big|\theta\Big].\end{aligned} \tag{44}$$

Using the trace operator and (32), (44) is given by

$$\begin{aligned}&\mathrm{D_{KL}}(f_{x|\theta}(x|\theta)||f_{x|\theta}(x|\alpha)) \\ &= \frac{\text{SNR}^2\ N}{1 + K\ \text{SNR}}\Big(K^2 - |a^H(Z,\theta)a(Z,\alpha)|^2\Big),\end{aligned} \tag{45}$$

where (45) depends on Z and α through $||a^H(Z,\theta)a(Z,\alpha)||_2^2$. The dependency of $||a^H(Z,\theta)a(Z,\alpha)||_2^2$ on Z and α is given

in (40), which is the same objective function defined as the ELL criterion in [39, Eq. (25a)].

APPENDIX F
CBCRB CRITERION FOR UCA

Let's assume a UCA design where the locations of the sensors are given by

$$z_k = r[\cos(\phi_k), \sin(\phi_k)], \tag{46}$$

where ϕ_k describes the locations of the equally spaced sensors around a circle of radius r,

$$\phi_k = \frac{2\pi(k-1)}{K}, \quad k = 1, \ldots, K. \tag{47}$$

Given the monotonic relation between the CBCRB and the periodic FIM as given in (13), the minimization in (23) is equivalent to maximizing the periodic FIM in (16). Since the maximization is w.r.t. Z, the non-negative term $\frac{N\,\mathrm{SNR}^2}{1+K\,\mathrm{SNR}}\left(\frac{2\pi}{\lambda}\right)^2$ can be omitted from the maximization of (16). Thus, the minimization in (23) is equivalent to maximizing the following w.r.t. Z:

$$J^{(p)} = \mathrm{Tr}\left(ZZ^T\right) - \frac{1}{K}\mathbf{1}^T ZZ^T \mathbf{1}. \tag{48}$$

For the UCA assumption, (48) can be written as

$$J^{(p)} = Kr^2 - \frac{1}{K}r^2 \sum_{k,l=1}^{K} \cos(\phi_k - \phi_l). \tag{49}$$

Since the locations are determined from a finite set of locations $\mathcal{Z}$, we will add a new constraint $r \le R$, where R is the largest radius possible from the optimal locations in $\mathcal{Z}$. We will show that (48) is non-negative:

$$r^2\left(K - \frac{1}{K}\sum_{k,l=1}^{K}\cos(\phi_k - \phi_l)\right) \ge r^2\left(K - \frac{K^2}{K}\right) = 0. \tag{50}$$

Thus, (49) is maximized for a maximal r, and (23) is given by

$$r_{\mathrm{CBCRB}} = \max\left\{r : \max_{\theta\in[-\pi,\pi)} \frac{1}{N_p}\sum_{m=1}^{N_p} P_m(r,\theta) \le \varepsilon_0(\mathrm{SNR})\right\}. \tag{51}$$

ACKNOWLEDGMENT

The authors would like to thank Dr. Yael Radzyner from the Soreq Nuclear Research Center for making a valuable contribution to the interactive discussion and for her supportive comments.

REFERENCES

[1] H. Krim and M. Viberg, "Two decades of array signal processing research: The parametric approach," *IEEE Signal Process. Mag.*, vol. 13, no. 4, pp. 67–94, Jul. 1996.
[2] P. Stoica and A. Nehorai, "Performance study of conditional and unconditional direction-of-arrival estimation," *IEEE Trans. Acoust., Speech, Signal Process.*, vol. 38, no. 10, pp. 1783–1795, Oct. 1990.
[3] H. L. Van Trees, *Optimum Array Processing: Part IV of Detection, Estimation, and Modulation Theory*. Hoboken, NJ, USA: Wiley, 2004.
[4] Y. Ma, X. Cao, X. Wang, M. S. Greco, and F. Gini, "Multi-source off-grid DOA estimation with single snapshot using non-uniform linear arrays," *Signal Process.*, vol. 189, Dec. 2021, Art. no. 108238.
[5] H. Wu, Q. Shen, W. Liu, and W. Cui, "Underdetermined low-complexity wideband DOA estimation with uniform linear arrays," in *Proc. IEEE 11th Sensor Array Multichannel Signal Process. Workshop (SAM)*, Jun. 2020, pp. 1–5.
[6] M. Khatib, Y. Ben-Horin, Y. Radzyner, J. D. Rosenblatt, and T. Routtenberg, "Periodic Fisher-scoring algorithm with applications for DOA estimation in seismic arrays," in *Proc. 26th Int. Conf. Inf. Fusion (FUSION)*, Jun. 2023, pp. 1–7.
[7] H. Zamani, H. Zayyani, and F. Marvasti, "An iterative dictionary learning-based algorithm for DOA estimation," *IEEE Commun. Lett.*, vol. 20, no. 9, pp. 1784–1787, Sep. 2016.
[8] S. Rost and C. Thomas, "Array seismology: Methods and applications," *Rev. Geophys.*, vol. 40, no. 3, pp. 1–2, Sep. 2002.
[9] J. H. McClellan, L. Eisner, E. Liu, N. Iqbal, A. A. Al-Shuhail, and S. I. Kaka, "Array processing in microseismic monitoring: Detection, enhancement, and localization of induced seismicity," *IEEE Signal Process. Mag.*, vol. 35, no. 2, pp. 99–111, Mar. 2018.
[10] A. H. Muqaibel, S. A. Alawsh, A. I. Oweis, and M. S. Sharawi, "Sparse DOA estimation for directional antenna arrays: An experimental validation," *IEEE Sensors J.*, vol. 21, no. 4, pp. 5173–5184, Feb. 2021.
[11] Y. Liu, H. Liu, X.-G. Xia, L. Wang, and G. Bi, "Target localization in multipath propagation environment using dictionary-based sparse representation," *IEEE Access*, vol. 7, pp. 150583–150597, 2019.
[12] Y. Liu, H. Liu, L. Wang, and G. Bi, "Target localization in high-coherence multipath environment based on low-rank decomposition and sparse representation," *IEEE Trans. Geosci. Remote Sens.*, vol. 58, no. 9, pp. 6197–6209, Sep. 2020.
[13] Y. Liu, Z.-W. Tan, A. W. H. Khong, and H. Liu, "An iterative implementation-based approach for joint source localization and association under multipath propagation environments," *IEEE Trans. Signal Process.*, vol. 71, pp. 121–135, 2023.
[14] Y. Liu, X.-G. Xia, H. Liu, A. H. T. Nguyen, and A. W. H. Khong, "Iterative implementation method for robust target localization in a mixed interference environment," *IEEE Trans. Geosci. Remote Sens.*, vol. 60, 2022, Art. no. 5107813.
[15] X. Cui, K. Yu, S. Zhang, and H. Wang, "Azimuth-only estimation for TDOA-based direction finding with 3-D acoustic array," *IEEE Trans. Instrum. Meas.*, vol. 69, no. 4, pp. 985–994, Apr. 2020.
[16] M. Heydariaan, H. Dabirian, and O. Gnawali, "AnguLoc: Concurrent angle of arrival estimation for indoor localization with UWB radios," in *Proc. 16th Int. Conf. Distrib. Comput. Sensor Syst. (DCOSS)*, May 2020, pp. 112–119.
[17] C. A. Langston, "Phased array analysis incorporating the continuous wavelet transform," *Bull. Seismological Soc. Amer.*, vol. 111, no. 5, pp. 2780–2798, Oct. 2021.
[18] S. Sun and A. P. Petropulu, "A sparse linear array approach in automotive radars using matrix completion," in *Proc. ICASSP - IEEE Int. Conf. Acoust., Speech Signal Process. (ICASSP)*, May 2020, pp. 8614–8618.
[19] D. Pearson, S. U. Pillai, and Y. Lee, "An algorithm for near-optimal placement of sensor elements," *IEEE Trans. Inf. Theory*, vol. 36, no. 6, pp. 1280–1284, Jun. 1990.
[20] Y. Zhao, Z. Li, B. Hao, and J. Shi, "Sensor selection for TDOA-based localization in wireless sensor networks with non-line-of-sight condition," *IEEE Trans. Veh. Technol.*, vol. 68, no. 10, pp. 9935–9950, Oct. 2019.
[21] M. Sadeghi, F. Behnia, and R. Amiri, "Optimal geometry analysis for TDOA-based localization under communication constraints," *IEEE Trans. Aerosp. Electron. Syst.*, vol. 57, no. 5, pp. 3096–3106, Oct. 2021.
[22] M. Hawkes and A. Nehorai, "Effects of sensor placement on acoustic vector-sensor array performance," *IEEE J. Ocean. Eng.*, vol. 24, no. 1, pp. 33–40, Jul. 1999.
[23] O. Lange and B. Yang, "Array geometry optimization for direction-of-arrival estimation including subarrays and tapering," in *Proc. Int. ITG Workshop Smart Antennas (WSA)*, Feb. 2010, pp. 135–142.

[24] O. Lange and B. Yang, "Antenna geometry optimization for 2D direction-of-arrival estimation for radar imaging," in *Proc. Int. ITG Workshop Smart Antennas*, Feb. 2011, pp. 1–8.
[25] U. Baysal and R. L. Moses, "On the geometry of isotropic arrays," *IEEE Trans. Signal Process.*, vol. 51, no. 6, pp. 1469–1478, Jun. 2003.
[26] U. Oktel and R. L. Moses, "A Bayesian approach to array geometry design," *IEEE Trans. Signal Process.*, vol. 53, no. 5, pp. 1919–1923, May 2005.
[27] H. Gazzah and S. Marcos, "Cramer-rao bounds for antenna array design," *IEEE Trans. Signal Process.*, vol. 54, no. 1, pp. 336–345, Jan. 2006.
[28] H. Gazzah and K. Abed-Meraim, "Optimum ambiguity-free directional and omnidirectional planar antenna arrays for DOA estimation," *IEEE Trans. Signal Process.*, vol. 57, no. 10, pp. 3942–3953, Oct. 2009.
[29] H. Gazzah and J.-P. Delmas, "Direction finding antenna arrays for the randomly located source," *IEEE Trans. Signal Process.*, vol. 60, no. 11, pp. 6063–6068, Nov. 2012.
[30] T. Birinci and Y. Tanık, "Optimization of nonuniform array geometry for DOA estimation with the constraint on gross error probability," *Signal Process.*, vol. 87, no. 10, pp. 2360–2369, Oct. 2007.
[31] A. B. Gershman and J. F. Bohme, "A note on most favorable array geometries for DOA estimation and array interpolation," *IEEE Signal Process. Lett.*, vol. 4, no. 8, pp. 232–235, Aug. 1997.
[32] R. Schmidt, "Multiple emitter location and signal parameter estimation," *IEEE Trans. Antennas Propag.*, vol. AP-34, no. 3, pp. 276–280, Mar. 1986.
[33] K. Beshara-Flynn and K. Adhikari, "Effects of signal and array parameters on MSE and CRB in DOA estimation," in *Proc. IEEE 13th Annu. Ubiquitous Comput., Electron. Mobile Commun. Conf. (UEMCON)*, Oct. 2022, pp. 0373–0379.
[34] P. Gupta and M. Agrawal, "Design and analysis of the sparse array for DoA estimation of noncircular signals," *IEEE Trans. Signal Process.*, vol. 67, no. 2, pp. 460–473, Jan. 2019.
[35] H. Gazzah and J.-P. Delmas, "Optimizing V antenna arrays using a Bayesian DOA estimation criterion," in *Proc. 1st Int. Conf. Commun., Signal Process., their Appl. (ICCSPA)*, Feb. 2013, pp. 1–6.
[36] F. Athley, "Threshold region performance of maximum likelihood direction of arrival estimators," *IEEE Trans. Signal Process.*, vol. 53, no. 4, pp. 1359–1373, Apr. 2005.
[37] H. Messer, "Source localization performance and the array beampattern," *Signal Process.*, vol. 28, no. 2, pp. 163–181, Aug. 1992.
[38] M. Gavish and A. J. Weiss, "Array geometry for ambiguity resolution in direction finding," *IEEE Trans. Antennas Propag.*, vol. 44, no. 6, pp. 889–895, Jun. 1996.
[39] S. Maranò, D. Fäh, and Y. M. Lu, "Sensor placement for the analysis of seismic surface waves: Sources of error, design criterion and array design algorithms," *Geophys. J. Int.*, vol. 197, no. 3, pp. 1566–1581, Apr. 2014.
[40] E. J. Vertatschitsch and S. Haykin, "Impact of linear array geometry on direction-of-arrival estimation for a single source," *IEEE Trans. Antennas Propag.*, vol. 39, no. 5, pp. 576–584, May 1991.
[41] R. A. Haubrich, "Array design," *Bull. Seismol. Soc. Amer.*, vol. 58, no. 3, pp. 977–991, Jun. 1968.
[42] H.-P. Harjes, "Design and siting of a new regional array in central Europe," *Bull. Seismolog. Soc. Amer.*, vol. 80, no. 6B, pp. 1801–1817, 1990.
[43] S. Mykkeltveit, K. Åstebøl, D. Doornbos, and E. Husebye, "Seismic array configuration optimization," *Bull. Seismolog. Soc. Amer.*, vol. 73, no. 1, pp. 173–186, 1983.
[44] Geophysical Institute of Israel. *IS: Israel National Seismic Network*. Accessed: Apr. 1, 2023. [Online]. Available: http://www.fdsn.org/networks/detail/IS/
[45] E. Nitzan, T. Routtenberg, and J. Tabrikian, "A new class of Bayesian cyclic bounds for periodic parameter estimation," *IEEE Trans. Signal Process.*, vol. 64, no. 1, pp. 229–243, Jan. 2016.
[46] E. Nitzan, T. Routtenberg, and J. Tabrikian, "Cyclic Bayesian Cramér–Rao bound for filtering in circular state space," in *Proc. 18th Int. Conf. Inf. Fusion (Fusion)*, 2015, pp. 734–741.
[47] B. A. Johnson and Y. I. Abramovich, "DOA estimator performance assessment in the pre-asymptotic domain using the likelihood principle," *Signal Process.*, vol. 90, no. 5, pp. 1392–1401, May 2010.
[48] E. T. Northardt, I. Bilik, and Y. I. Abramovich, "Spatial compressive sensing for direction-of-arrival estimation with bias mitigation via expected likelihood," *IEEE Trans. Signal Process.*, vol. 61, no. 5, pp. 1183–1195, Mar. 2013.
[49] N. Zimerman, J. D. Rosenblatt, and T. Routtenberg, "Colored noise in DOA estimation from seismic data: An empirical study," in *Proc. 54th Asilomar Conf. Signals, Syst. Comput.*, 2020, pp. 1240–1244.
[50] N. D. Selby, "Improved teleseismic signal detection at small-aperture arrays," *Bull. Seismolog. Soc. Amer.*, vol. 101, no. 4, pp. 1563–1575, Aug. 2011.
[51] S. M. Kay, *Fundamentals of Statistical Signal Processing: Practical Algorithm Development*, vol. 3. London, U.K.: Pearson, 2013.
[52] J. P. Delmas, "Performance bounds and statistical analysis of DOA estimation," in *Academic Press Library in Signal Processing*. Amsterdam, The Netherlands: Elsevier, 2014, pp. 719–764.
[53] T. Routtenberg and J. Tabrikian, "Bayesian parameter estimation using periodic cost functions," *IEEE Trans. Signal Process.*, vol. 60, no. 3, pp. 1229–1240, Mar. 2012.
[54] E. Weinstein and A. J. Weiss, "A general class of lower bounds in parameter estimation," *IEEE Trans. Inf. Theory*, vol. 34, no. 2, pp. 338–342, Mar. 1988.
[55] M. Ibrahim, V. Ramireddy, A. Lavrenko, J. König, F. Römer, M. Landmann, M. Grossmann, G. Del Galdo, and R. S. Thomä, "Design and analysis of compressive antenna arrays for direction of arrival estimation," *Signal Process.*, vol. 138, pp. 35–47, Sep. 2017.
[56] I. S. Gradshteyn and I. M. Ryzhik, *Table of Integrals, Series, and Products*. New York, NY, USA: Academic, 2014.
[57] M. Häge and M. Joswig, "Mapping local microseismicity using short-term tripartite small array installations—Case study: Coy region (SE Spain)," *Tectonophysics*, vol. 471, nos. 3–4, pp. 225–231, Jun. 2009.
[58] F. Belloni and V. Koivunen, "Beamspace transform for UCA: Error analysis and bias reduction," *IEEE Trans. Signal Process.*, vol. 54, no. 8, pp. 3078–3089, Aug. 2006.
[59] R. Goossens and H. Rogier, "A hybrid UCA-RARE/root-MUSIC approach for 2-D direction of arrival estimation in uniform circular arrays in the presence of mutual coupling," *IEEE Trans. Antennas Propag.*, vol. 55, no. 3, pp. 841–849, Mar. 2007.
[60] T. Filik and T. E. Tuncer, "Uniform and nonuniform V-shaped isotropic planar arrays," in *Proc. 5th IEEE Sensor Array Multichannel Signal Process. Workshop*, Jul. 2008, pp. 99–103.
[61] K. Petersen and M. Pedersen, "The matrix cookbook, version 20121115," Tech. Univ. Denmark, Kongens Lyngby, Denmark, Tech. Rep. 3274, 2012. [Online]. Available: http://www2.compute.dtu.dk/pubdb/pubs/3274-full.html
[62] A. J. Weiss and B. Friedlander, "On the Cramer RAO bound for direction finding of correlated signals," in *Proc. Conf. Rec. 24th Asilomar Conf. Signals, Syst. Comput.*, 1990, p. 941.
[63] D. J. MacKay and D. J. Mac Kay, *Information Theory, Inference and Learning Algorithms*. Cambridge, U.K.: Cambridge Univ. Press, 2003.

NETA ZIMERMAN KATZ received the B.Sc. degree (cum laude) in biomedical engineering from the Technion—Israel Institute of Technology, Israel, in 2018, and the M.Sc. degree in electrical and computer engineering from the Ben-Gurion University of the Negev, Israel, in 2021. She is currently an Algorithm Engineer with Mobileye. At the time of this research, she was affiliated with the School of Electrical Engineering, Ben-Gurion University. She was awarded the Alfred and Anna Grey Scholarship, in 2014 and 2018, and Israel Ministry of National Infrastructure, Energy, and Water Scholarship in engineering and exact science, in 2020.

MALAAK KHATIB (Student Member, IEEE) received the B.Sc. degree in electrical and computer engineering from the Ben-Gurion University of the Negev, Be'er Sheva, Israel, in 2022, where she is currently pursuing the M.Sc. degree with the School of Electrical and Computer Engineering. She was awarded the Paul and Edwina Heller and the Silins Foundation Scholarship, in 2022, Israeli Council for Higher Education Scholarship, in 2022, and the Goldman Sonnenfeldt School of Sustainability and Climate Change Scholarship, in 2023. Her research interests include statistical signal processing, parameter estimation under model misspecification, and periodic parameter estimation with application to seismic azimuth estimation for seismic arrays.

YOCHAI BEN-HORIN received the D.Sc. degree in theoretical physics from the Technion—Israel Institute of Technology, Haifa, in 1997. Since 1998, he has been a Researcher with the National Data of Israel, Soreq Nuclear Research Center.

JONATHAN D. ROSENBLATT received the Ph.D. degree in statistics from Tel Aviv University. He was a Senior Lecturer with the Faculty of Engineering, Ben-Gurion University of the Negev, between 2015 and 2021. He is currently a Data Scientist with Fairmatic, an insure-tech company.

TIRZA ROUTTENBERG (Senior Member, IEEE) received the B.Sc. degree from the Technion—Israel Institute of Technology, Haifa, Israel, in 2005, and the M.Sc. and Ph.D. degrees in electrical and computer engineering from the Ben-Gurion University of the Negev, Be'er Sheva, Israel, in 2007 and 2012, respectively. She is currently an Associate Professor with the School of Electrical and Computer Engineering, Ben-Gurion University of the Negev. She was a Postdoctoral Fellow with the School of Electrical and Computer Engineering, Cornell University, from 2012 to 2014. Since October 2014, she has been a Faculty Member of the School of Electrical and Computer Engineering, Ben-Gurion University of the Negev. In 2022 and 2023, she was a William R. Kenan, Jr. Visiting Professor for Distinguished Teaching with Princeton University. Her research interests include statistical signal processing with applications in sensor arrays and energy systems. She is an Associate Editor of IEEE TRANSACTIONS ON SIGNAL AND INFORMATION PROCESSING OVER NETWORKS and IEEE SIGNAL PROCESSING LETTERS, and a member of the IEEE Signal Processing Theory and Methods Technical Committee. She was a recipient of the Best Student Paper Award at ICASSP 2011, CAMSAP 2013 (the coauthor), ICASSP 2017 (the coauthor), and SSP 2018 (the coauthor). She was awarded the Negev Scholarship, in 2008, the Lev-Zion Scholarship, in 2010, the Marc Rich Foundation Prize, in 2011, and Toronto Prize for Excellence in Research, in 2021.